Mineralogical Magazine, February 2013, Vol. 77(1), pp. 45–55

Kleberite, $\mathrm{Fe^{3+}Ti_6O_{11}(OH)_5}$, a new ilmenite alteration product, from Königshain, northeast Germany

I. E. GREY[1],*, K. STEINIKE[2] AND C. M. MACRAE[1]

[1] CSIRO Process Science and Engineering, Box 312, Clayton South, Victoria 3169, Australia
[2] Waldstrasse 8, OT Grunau, DE 12527 Berlin, Germany

[*Received 2 October 2012; Accepted 13 December 2012; Associate Editor: Giancarlo Della Ventura*]

ABSTRACT

Kleberite, ideally $\mathrm{Fe^{3+}Ti_6O_{11}(OH)_5}$, is a new mineral (IMA 2012-023) from Tertiary sands at Königshain, Saxony, northeast Germany. It is also found in heavy mineral sands from the Murray Basin, southeast Australia and at Kalimantan, Indonesia. It occurs as rounded anhedral to euhedral translucent grains, 0.04–0.3 mm across, which are generally red-brown, but grade to orange with decreasing iron content. Associated minerals include ilmenite, pseudorutile, 'leucoxene', tourmaline and spinel. The density measured by pycnometry is 3.28 g cm^{-3}, which is lower than the calculated density of 3.91 g cm^{-3}, due to intragrain porosity which is not penetrated by the immersion fluid. The intragrain pores, of median diameter 18 nm, are partially filled with impurity phases including kaolinite, diaspore and quartz. Kleberite grains have a uniaxial (–) character, but localized regions are weakly biaxial (–) with 2V close to zero. The mean refractive index, calculated from reflectance measurements, is 2.16(3). The mean empirical formula from electron-microprobe analyses of 15 Königshain kleberite grains is $\mathrm{Fe^{3+}_{1.01}Mg_{0.06}Ti_6O_{11.2}(OH)_{4.8}[Al_{0.59}Si_{0.31}P_{0.04}O_{1.60}{\cdot}1.8H_2O]}$, where the formula element in square brackets represents impurities in the pores. Kleberite forms over a compositional range with [Ti]/[Fe + Ti] atomic ratios from 0.8–0.9. It has monoclinic symmetry, $P2_1/c$, with a = 7.537(1), b = 4.5795(4), c = 9.885(1) Å, β = 131.02(1)°. The six strongest lines in the powder X-ray diffraction (XRD) pattern [listed as d in Å (I)] are as follows: 1.676(100), 2.170(82), 2.466(27), 1.423(22), 3.933(8), 2.764(9). The structure was refined by the Rietveld method on powder XRD data to R_p = 6.3, R_wp = 8.1, R_B = 4.0. Kleberite is isostructural with tivanite; their structural formulae are $\mathrm{[Ti^{4+}_3\square][Ti^{4+}_3Fe^{3+}]O_{11}(OH)_5}$ and $\mathrm{[Ti^{4+}_4][V^{3+}_4]O_{12}(OH)_4}$, respectively. Kleberite has dominant Ti^{4+} in place of V^{3+} in the M(2) metal-atom site. The related mineral pseudorutile, $\mathrm{[Ti_4][(Fe^{3+},Ti)_4](O,OH)_{16}}$, with Fe^{3+} > Ti^{4+} has dominant Fe^{3+} in this site. Kleberite grains from different localities commonly contain residual MgO-rich ferrian ilmenite. The chemical and physical relationships between the ilmenite and coexisting kleberite are used to evaluate different alteration mechanisms involving selective leaching of divalent oxides from ilmenite and pseudomorphic replacement reactions, respectively.

KEYWORDS: new mineral, kleberite, pseudorutile, Rietveld refinement, ilmenite alteration, selective leaching of MgO-rich ferrian ilmenite, tivanite-type structure, pseudomorphic replacement reaction.

Introduction

KLEBERITE was first found in 1963 (by KS) in heavy mineral fractions derived from the Tertiary sands and gravels of northeast Germany. The mineral grains were distinguished from other heavy minerals by their striking red-brown translucent appearance. During the next decade or so, the mineral was identified as a rare but persistent component in heavy mineral fractions analysed at the Zentrales

---

* E-mail: ian.grey@csiro.au
DOI: 10.1180/minmag.2013.077.1.05

© 2013 The Mineralogical Society

Geologisches Institut, Berlin, from samples collected over an extensive area (>20,000 km^2) of northeast Germany as part of a uranium exploration project (Steinike, 2008). The project was confidential, and the discovery was not made public until 1978, when the mineral was described by Bautsch *et al*. (1978) and given the name kleberite (without IMA approval). Optical examination of sectioned grains revealed ilmenite cores in some grains, suggesting that kleberite formed by the alteration of ilmenite (Bautsch *et al*., 1978). Kleberite grains have markedly lower iron contents and higher water contents (by a factor of ~3) than those reported for the ilmenite alteration phase pseudorutile (Grey and Reid, 1975).

Kleberite was subsequently identified in heavy mineral sand concentrates from the Murray Basin, southeast Australia (Grey and Li, 2003) and from Kalimantan, Indonesia (Grey *et al*., 2010). In both cases the mineral was referred to as hydroxylian pseudorutile, because of the similarity of the powder X-ray diffraction (XRD) patterns and the high content of strongly held water (hydroxyls). A detailed crystallographic study of the Kalimantan sample (Grey *et al*., 2010) built on earlier studies (Grey *et al*., 1983) and showed kleberite to be a structural analogue of tivanite, $V^{3+}TiO_3OH$ (Grey and Nickel, 1981) with dominant Ti^{4+} rather than V^{3+} in the M(2) metal-atom site. This also distinguishes it from pseudorutile, which has dominant Fe^{3+} in this site.

We have recently remeasured the chemical, thermal and XRD properties of kleberite grains from northeast Germany and have confirmed their close similarity to those of samples from the Murray Basin and from Kalimantan. The mineral and name have been approved by the IMA Commission of New Minerals, Nomenclature and Classification (IMA 2012-023). Kleberite is named in honour of Dr Will Kleber (1906−1970), a former director of the Institute of Mineralogy and the Museum of Mineralogy at Humboldt University, Berlin, for his seminal contributions to crystallography research and education, and for his major research contributions in the fields of crystal growth, epitaxy and topotaxy. Type material from Königshain, Saxony, Germany is catalogued in the mineral collection of the Museum für Naturkunde, Humboldt University, Berlin, Germany, under inventory number 1980-0283. Cotype specimens of kleberite from the Murray Basin and Kalimantan are preserved in the collections of Museum Victoria, Melbourne, Victoria, Australia, under registration numbers M52010 and M52011.

Occurrence

Kleberite is widely distributed in Tertiary sands and gravels in northeast Germany. Steinike (2008) documented more than 40 localities in a 20,000 km^2 region bounded by Berlin in the north, Zwickau in the south, Cottbus in the east and Magdeburg in the west, where mineralogical analysis of the heavy mineral fraction of exploration samples showed the presence of kleberite. It is particularly concentrated in alluvial sands close to Roda (51º3′N 12º37′E) and Königshain (50º58′N 12º53′E) in Saxony (Steinike, 2008). Kleberite has also been identified in heavy mineral sand concentrates from the Murray Basin, southeast Australia (Grey and Li, 2003) and from Kalimantan, Indonesia (Grey *et al*., 2010). The German and Australian localities were inland seas during the Tertiary period and the heavy minerals were fed into the marine basins during the Miocene/Pliocene epochs. The source of kleberite in northeast Germany is likely to be the basalts of the Erzgebirge mountains, on the border between Saxony and the Czech Republic (Steinike, 2008). Fluvial action transported mineral grains eroded from the mountains into the marine basin south of Berlin.

Ilmenite, pseudorutile, 'leucoxene', tourmaline and spinel are present in the heavy mineral concentrates at all three localities. The kleberite grains commonly contain inclusions and intrapore deposits of very fine-grained kaolinite, quartz and diaspore, as well as residual ilmenite. A feature common to the three localities is that the residual unweathered ilmenite within the kleberite grains has a relatively constant MgO-rich ferrian composition.

Appearance and physical properties

Kleberite occurs as rounded anhedral to euhedral translucent grains of a red-brown colour. The colour of kleberite grains from the Murray Basin and Kalimantan grades from red-brown to orange with decreasing iron content. The translucence of the grains contrasts with other weathering products of ilmenite, specifically pseudorutile and secondary rutile, which are opaque (see fig. 1 in Grey and Li, 2003). Grain sizes range from ~0.04 to 0.3 mm. The grains are pseudomorphous after ilmenite and commonly

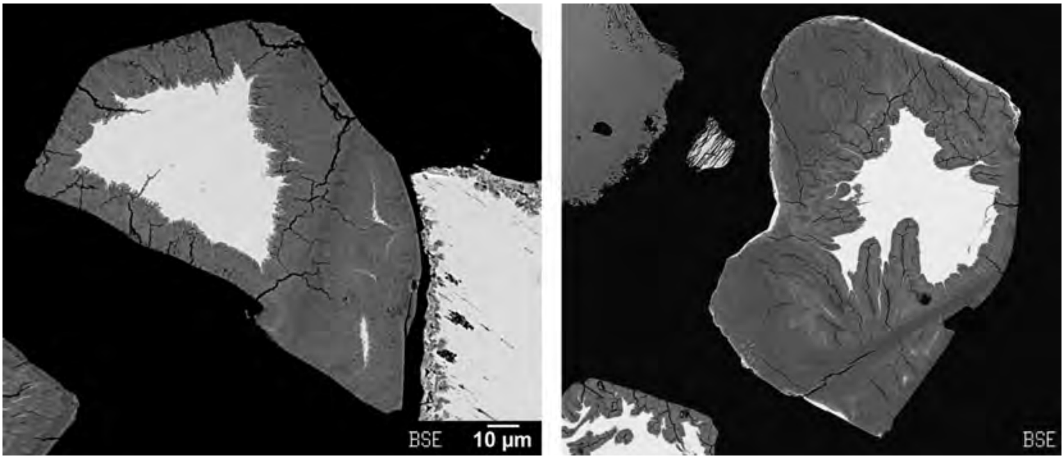

FIG. 1. Back-scattered electron photomicrographs of kleberite grains containing unaltered residual MgO-rich ferrian ilmenite cores.

retain the hexagonal tabular form of the parent mineral. Residual MgO-bearing ferrian ilmenite is found in some kleberite grains (Fig. 1).

The grains have a waxy to vitreous appearance and a beige-coloured streak. They are relatively brittle with an irregular fracture. The measured density (using pycnometry; Bautsch *et al*. 1978) is 3.28 g cm^{-3} for Königshain kleberite. Grains from the Murray Basin and Kalimantan float in diiodomethane (which has a density of 3.31 g cm^{-3}) and sink in tetrabromoethane (which has a density of 2.97 g cm^{-3}), and they therefore have densities which are consistent with the measured density of Königshain kleberite. The calculated density, based on the formula $FeTi_6O_{11}(OH)_5$ and unit-cell parameters is 3.91 g cm^{-3}. The low measured density is due to nanoscale intragrain porosity which is not penetrated by density fluids. Mercury porosimetry measurements have confirmed the nanoporosity. Grains from a NSW deposit in the Murray Basin have a porosity of 0.04 cm^3 g^{-1} and the pores have a median diameter of 18 nm. A nitrogen gas Brunauer–Emmett–Teller (BET) measurement of specific surface area gave a value of 26 m^2 g^{-1} (Grey and Li, 2003).

The thermogravimetric (TG) and differential thermal analysis (DTA) properties of Konigshain kleberite were measured using a Seteram Setsys Evolution Simultaneous TGA/DTA Thermal Analyser system, coupled to a Pfeiffer mass spectrometer to analyse the gases evolved. A 14 mg sample of crushed grains was placed in an alumina crucible and heated from ambient temperature to 800ºC in a flow of high purity argon, at a rate of 10ºC min^{-1}. The DTA and TG curves are shown in Fig. 2. The experiment revealed that water was the dominant evolved gas, as shown by the MS curve for atomic mass 18 in Fig. 2; CO_x and SO_x species were also detected, at peak temperatures of ~500ºC and 780ºC, respectively, but the ion currents were two to three orders-of-magnitude smaller than those for H_2O. Over 90% of the mass loss of 10.6 wt.% occurs in the temperature range 50−600ºC, with the highest rate of mass loss between 250 and 300ºC. The broad associated endotherm shows resolved maxima at 90, 170, 230 and 270ºC. The endotherm at 700ºC corresponds to SO_3 evolution, but the associated mass loss is very small at this temperature. Thermogravimetric analyses of Murray Basin kleberite (Grey and Li, 2003) and Kalimantan kleberite are reported in Grey and Li (2003) and Grey *et al*. (2010), respectively. The thermal properties of kleberite grains from the three localities are similar. Loss of water over an extended temperature range has been reported for pseudorutile (Grey and Li, 2003), but the total mass loss is only about one third of that measured for kleberite.

Optical properties

Kleberite grains from northeast Germany have a uniaxial (−) character. Local regions of the grains are weakly biaxial (−) with 2V close to zero. The birefringence (measured by conoscopy) is 0.04 to 0.05 (Bautsch *et al*., 1978). In transmitted light,

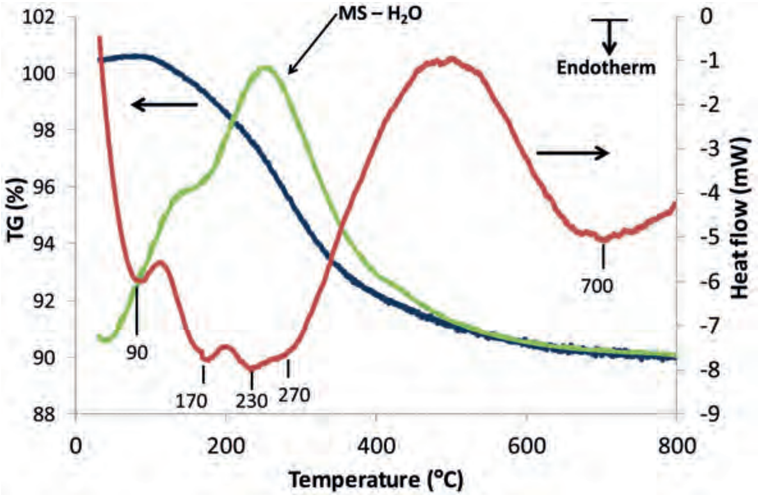

FIG. 2. The TG and DTA curves for Königshain kleberite and the ion current MS curve for atomic mass 18 (i.e. H_2O).

kleberite grains are slightly cloudy, with colours ranging from yellow through red-brown to deep red, and fine-grained to fine-spindle form dark internal structure. Rhythmic zoning is common, and was found to be due to small (1–2 wt.%) variations in the iron content. In reflected light the grains appear isotropic with weak dark blue-grey reflectivity.

The refractive indices of kleberite are greater than 2, and therefore beyond the range of refractive index fluids. Their values could not be determined by conventional immersion techniques. Instead, reflectance measurements were made on 23 grains using a Velomet Interphako VEB Carl Zeiss microscope with unpolarized light (Bautsch *et al*., 1978). The refractive indices were calculated from the reflectance values; 93% of the indices lie between 2.090 and 2.225, with 43% of the values in the range 2.135 to 2.175. The mean calculated refractive index is 2.16(3). The optical properties of kleberite grains from the northeast Germany and Murray Basin localities were compared at the Institute for Geosciences at Kiel University in 2007 (Steinike and Kaemmel, 2008) and found to be essentially identical, with grains from both localities displaying the same reddish colour, high refractive indices and uniaxial (–) character.

Chemical composition

Grains of Königshain kleberite were mounted in an epoxy block and polished for electron-microprobe (EMP) analyses, which were conducted using a JEOL Hyperprobe JXA-8500F in wavelength-dispersive spectrometry mode. The operating conditions were 15 kV and 18 nA with the beam defocussed to 5 μm. Standards used were synthetic $MgAl_2O_4$ (Mg, Al), $MnSiO_3$ (Mn), $AlPO_4$ (P), YVO_4 (V), and the minerals hematite (Fe), rutile (Ti) and wollastonite (Si).

The results of analyses of 15 grains are given in Table 1, where they are compared with EMP analyses of Murray Basin kleberite (Grey and Li, 2003) and Kalimantan kleberite (Grey *et al*., 2010), and with X-ray fluorescence analyses of neotype pseudorutile from Neptune Island, South Australia (Grey *et al*., 1994). The kleberite analyses differ significantly from the pseudorutile analyses in having less than one third of the iron oxide content, more than three times the water content and considerably larger amounts of SiO_2, Al_2O_3 and P_2O_5. The three kleberite samples have similar compositions, except for the unusually high Al content of the Kalimantan sample. Detailed studies were made of the mode of incorporation of Al in this sample, using EMP analyses of 500 separate grains, synchrotron powder XRD, differential pair distribution function analysis and ^{27}Al MAS NMR spectroscopy (Grey *et al*., 2010). The results are consistent with the Al being incorporated within fine pores in the kleberite grains, as nanoscale crystals of diaspore, AlOOH (which is probably also Fe-bearing).

TABLE 1. Analyses (wt.%) for kleberite from three localities and neotype pseudorutile.

	Königshain, northeast Germany EMP + TGA (Mean of 15 grain analyses)			[1]Murray Basin EMP + TGA (300 grains)	[2]Kalimantan EMP + TGA (486 grains)	[1]Pseudorutile Neptune Is. XRF + TGA
Constituent	Mean	Range	SD	Mean	Mean	Mean
TiO_2	65.9	59.0–70.1	3.3	69.3	61.6	58.3
Fe_2O_3	11.2	9.0–15.9	1.9	10.3	10.4	34.6
Al_2O_3	4.20	2.04–7.86	1.7	2.5	11.4	0.38
SiO_2	2.57	1.48–3.12	0.46	1.7	1.16	0.36
P_2O_5	0.51	0.21–0.98	0.22	0.41	0.54	0.15
V_2O_5	0.50	0–0.88	0.26	0.30	0.70	0.18
MnO	0.07	0–0.15	0.06	0.21	0.10	0.58
MgO	0.31	0.15–0.50	0.12	0.46	0.20	0.33
H_2O	10.6			10.9	11.8	3.2
Total	95.9			96.1	97.9	98.1

[1] Grey and Li (2003), [2] Grey *et al*. (2010).

More generally, isovolumetric alteration of ilmenite grains to form kleberite (or pseudorutile) results in the formation of a fine network of pores in the chemically weathered grains as confirmed by the porosimetry results. Impurity minerals are incorporated from the groundwater environment into the pores, or are adsorbed onto the pore walls (Frost *et al*., 1983). Anand and Gilkes (1984, 1985) have used transmission electron microscopy/electron diffraction to observe submicrometre-sized crystals of halloysite, kaolinite and gibbsite in the <5 μm fraction of crushed grains of highly weathered ilmenite. They suggest that they come from intragrain pores. We have observed weak peaks due to diaspore, quartz and kaolinite in the powder XRD patterns produced by different kleberite samples.

In calculating the formulae of the kleberite samples from the analyses in Table 1, we have separated the titanate matrix components from the components that are present in the pores (i.e. SiO_2, Al_2O_3, P_2O_5, H_2O). The minor elements Mg, Mn and V are present in the parent ilmenite and are expected to be retained in the matrix structure. Trace amounts of Mn and V are incorporated into the Mg and Fe contents, respectively. The titanate matrix is normalized to 6 Ti and 16 (O + OH) anions per formula unit, to be consistent with the crystal structure results, with the O:OH ratio adjusted to maintain charge balance. This gives the following formulae, with the intrapore impurity compositions shown in square brackets:

Königshain kleberite: $Fe^{3+}_{1.01}Mg_{0.06}Ti_6O_{11.2}(OH)_{4.8}[Al_{0.59}Si_{0.31}P_{0.04}\ O_{1.60}\cdot 1.8H_2O]$

Murray Basin kleberite: $Fe^{3+}_{0.89}Mg_{0.10}Ti_6O_{10.9}(OH)_{5.1}[Al_{0.34}Si_{0.19}P_{0.04}O_{0.99}\cdot 1.6H_2O]$

Kalimantan kleberite: $Fe^{3+}_{1.00}Mg_{0.04}Ti_6O_{11.1}(OH)_{4.9}[(AlOOH)_{1.8}Si_{0.15}P_{0.06}O_{0.45}\cdot 1.7H_2O]$

The matrix compositions of the kleberite samples from the three localities are similar, and can be expressed by the simplified formula $Fe^{3+}Ti^{4+}_6O_{11}(OH)_5$.

Crystallography

Kleberite powder XRD patterns are very similar to the patterns for pseudorutile (see fig. 6, Grey and Li, 2003). They contain relatively sharp pseudohexagonal subcell peaks due to a hexagonal close-packed anion lattice, plus broader superlattice peaks due to metal atom ordering. The subcell peaks can be indexed on a hexagonal cell with $a = 2.845(1)$, $c = 4.575(1)$ Å for kleberite (Murray Basin) and $a = 2.866(1)$, $c = 4.602(1)$ Å for neotype pseudorutile (Grey and Li, 2003). The peak widths show that the domain size for ordering of the anion sublattice is ~20 nm, whereas the metal atom ordering is restricted to domains that are only a few nanometres in size. A model was originally developed for pseudorutile, based on a 5*a* hexagonal superlattice, for metal atom ordering (Grey and Reid, 1975). The model was refined to $R = 0.069$ using single-crystal intensity data collected on a single grain. The hexagonal model was unsatisfactory in that the hexagonal superlattice reflection positions corresponded to a non-integral multiple (5.26) of the subcell *a* lattice parameter, which was approximated to 5. In the refinement a number of the sites had partial occupancies.

A breakthrough in the structure analysis occurred when it was found that the single-grain diffraction patterns produced by pseudorutile were similar to those for multiply twinned tivanite, with arcs of diffuse intensity in pseudorutile having the same loci as clusters of twin spots in tivanite (Grey and Nickel, 1981). Pseudorutile and kleberite could then be considered as microtwinned analogues of tivanite. This model was successfully tested using synchrotron powder XRD data collected on the Kalimantan kleberite sample (Grey *et al*., 2010). In the current study we have tested the model against the powder XRD data for Königshain kleberite. A Rietveld powder XRD data collection was made on finely ground Königshain kleberite grains dispersed using ethanol on a zero-background plate (silicon disc). Intensity data were obtained using a Philips diffractometer equipped with a graphite monochromator and employing Cu*K*α radiation. Operating conditions were 40 kV and 40 mA, with 1º divergence and scatter slits, a 0.3 mm receiving slit and collimation by Soller slits. Step-scan intensity data were collected in the 2θ range 15 to 100º, using a step size of 0.02º and a counting time of 8 s. Rietveld refinements were conducted with *FULLPROF* software (Rodriguez-Carvajal, 1990).

The atom coordinates (Grey and Nickel, 1981) for tivanite from a single-crystal refinement in space group $P2_1/c$ were used as starting coordinates. Separate halfwidth parameters were used for the sharp subcell reflections and the broad metal-ordering reflections. As a result of the limited number of non-overlapping reflections, the atom parameters that were refined were restricted to the metal-atom coordinates and site occupancies, and isotropic displacement parameters for the metal atoms and for the oxygen atoms. Refinement of profile parameters, unit-cell parameters and atom parameters converged to $R_p = 6.3\%$, $R_{wp} = 8.1\%$, $R_B = 4.0\%$. The refinement results are given in Table 2. The calculated and observed diffraction patterns are compared in Fig. 3. The indexed powder XRD pattern for Königshain kleberite is given in Table 3.

A polyhedral representation of the kleberite structure, viewed at a small angle to [101], is shown in Fig. 4. In the (010) planes, the octahedra link by edge-sharing to form stepped chains along [101] and the chains are connected by corner-sharing along [010]. The structure can be described as a unit-cell scale intergrowth of goethite-type M(2)O(OH) (with M(2) occupied by V^{3+} in tivanite) and rutile-type $M(1)O_2$ structural elements (Grey and Nickel, 1981). The intergrowth plane is parallel to (100). As shown in Table 2, the occupancies of the M(1) and M(2) sites are [0.73(1)Ti + 0.27(1)□] and [0.74Ti + 0.26Fe], respectively. The corresponding formula, with the O:OH ratio adjusted for charge balance is $Fe^{3+}_{1.04}Ti_{5.88}O_{10.64}(OH)_{5.36}$, which is very similar to the matrix formula derived from the chemical analyses.

The ideal structural formulae for tivanite, kleberite and pseudorutile, with the contents of the M(1) and M(2) sites shown explicitly in square brackets are as follows:

TABLE 2. Rietveld refinement of the tivanite model in $P2_1/c$ for Konigshain kleberite.

Atom	Wyckoff Site	Occupancy	*x*/*a*	y/*b*	z/*c*	*B* (Å^2)
M1	4e	0.73(1)Ti + 0.27□	0.117(4)	0.039(3)	0.193(2)	1.51(4)
M2	4e	0.74Ti + 0.26Fe	0.323(1)	0.018(4)	0.567(1)	1.51(4)
O1	4e	1.0 O	0.134	0.238	0.355	1.6(1)
O2	4e	1.0 O	0.390	0.239	0.750	1.6(1)
O3	4e	1.0 O	0.636	0.273	0.107	1.6(1)
O4	4e	1.0 O	0.866	0.263	0.459	1.6(1)

The monoclinic unit cell has *a* = 7.537(1), *b* = 4.5795(4), *c* = 9.885(1) Å, β = 131.02(1)º.
The anion sublattice hexagonal cell has *a* = 2.850, *c* = 4.579 Å.
Refinement indices are as follows: $R_p = 6.3$, $R_{wp} = 8.1$, $R_B = 4.0$.

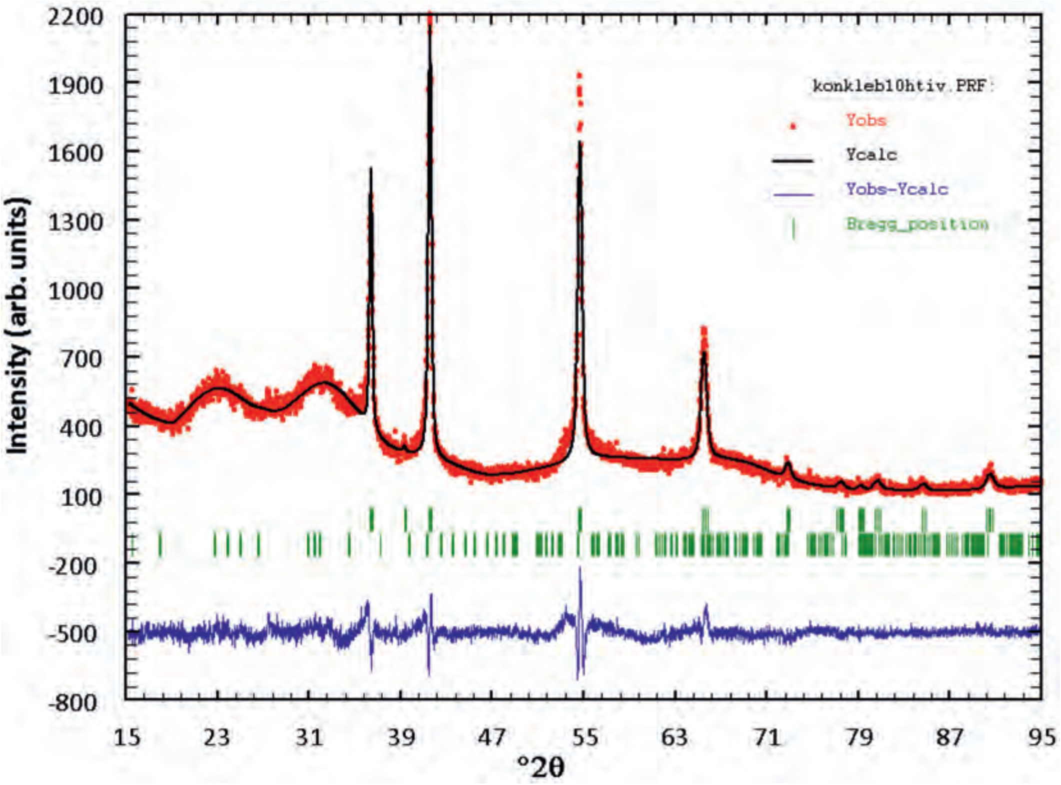

FIG. 3. Observed (dots) and calculated (line) powder XRD pattern for Königshain kleberite. The difference plot is shown below. The upper tick marks correspond to Bragg reflection positions for the hexagonal subcell reflections, whereas the lower tick marks indicate the metal-ordering reflection positions in the monoclinic cell.

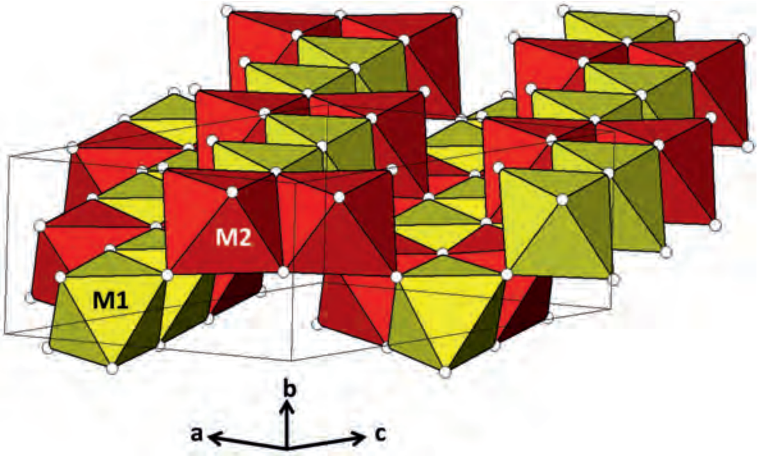

FIG. 4. Polyhedral representation of the kleberite structure, viewed approximately along [101]. The locations of the two metal-atom sites, M(1) and M(2), are shown.

TABLE 3. X-ray powder diffraction data for kleberite from Königshain.

I_{obs}	d_{obs}	d_{calc}	h	k	l
8(br)	**3.933**	3.902	0	1	1
		3.903	$\bar{1}$	1	1
9(br)	**2.764**	2.801	$\bar{2}$	1	1
		2.603	$\bar{1}$	1	3
27	**2.466**	2.464	1	0	2
		2.465	$\bar{3}$	0	2
		2.471	$\bar{2}$	0	4
82	**2.170**	2.170	1	1	2
		2.171	$\bar{3}$	1	2
		2.175	$\bar{2}$	1	4
100	**1.676**	1.678	1	2	2
		1.678	$\bar{3}$	2	2
		1.679	$\bar{2}$	2	4
4(br,sh)	1.624	1.637	$\bar{4}$	1	5
		1.611	$\bar{3}$	2	4
22	**1.423**	1.422	4	0	0
		1.425	$\bar{1}$	0	6
4(br,sh)	1.392	1.402	$\bar{2}$	3	1
		1.389	$\bar{5}$	1	3
6	1.297	1.298	1	3	2
		1.299	$\bar{2}$	3	4
1	1.234	1.244	$\bar{6}$	0	6
		1.232	2	0	4
1	1.207	1.208	$\bar{5}$	0	8
2	1.191	1.190	2	1	4
		1.193	$\bar{4}$	1	8
	1.144	1.151	0	4	0
		1.149	$\bar{4}$	3	5
1(br,sh)	1.097	1.105	3	3	1
		1.093	$\bar{6}$	2	6
6	1.085	1.085	2	2	4
3	1.038	1.038	1	4	2
		1.037	2	1	5
		1.033	$\bar{7}$	0	4

The six strongest lines in the pattern are listed in bold.

Tivanite: $[\mathrm{Ti}_4^{4+}][\mathrm{V}_4^{3+}]\mathrm{O}_{12}(\mathrm{OH})_4$
Kleberite: $[\mathrm{Ti}_3^{4+}\square]\ [\mathrm{Ti}_3^{4+}\mathrm{Fe}^{3+}]\mathrm{O}_{11}(\mathrm{OH})_5$
Pseudorutile: $[\mathrm{Ti}_4^{4+}][(\mathrm{Fe}^{3+},\mathrm{Ti}^{4+})_4](\mathrm{O},\mathrm{OH})_{16}$

Kleberite is thus a Ti-dominant analogue of tivanite, with Ti^{4+} and some Fe^{3+} replacing V^{3+} in the M(2) site. Charge balance is maintained by vacancies in the Ti-dominated M(1) site and a small change in the O:OH ratio. Kleberite is distinct from pseudorutile, which is an Fe^{3+}-dominant analogue of tivanite with $\mathrm{Fe}^{3+}>\mathrm{Ti}^{4+}$ in the M(2) site. The three minerals are isostructural. It should be emphasized that the formulae given for kleberite and pseudorutile correspond to the average matrix compositions. Both minerals have relatively wide compositional ranges, with variable Fe:Ti ratios, as illustrated by the range of analyses for Königshain kleberite in Table 1. Typical ranges for the [Ti]/[Fe + Ti] atomic ratio for pseudorutile and kleberite are 0.6 to 0.7, and 0.8 to 0.9, respectively (Frost *et al*., 1983; Grey and Li, 2003).

Mechanism for kleberite formation

A feature which is common to kleberite grains from the three different localities is the presence of residual unweathered MgO-rich ferrian ilmenite (Fig. 1). The EMP analyses of coexisting ilmenite and kleberite in composite grains can be used to help develop a mechanism for kleberite formation. We have analysed residual ilmenite and associated kleberite in composite Königshain kleberite grains, examples of which are given in Table 4. The average ilmenite composition from the six analyses is $(\mathrm{FeTiO_3})_{0.67}(\mathrm{MgTiO_3})_{0.17}(\mathrm{MnTiO_3})_{0.02}(\mathrm{Fe_2O_3})_{0.14}$. An almost identical mean composition was found for residual ilmenite in kleberite grains from the Murray Basin (Grey and Li, 2003).

In the context of developing a formation mechanism, an important correlation in the results listed in Table 4 is between the mole fraction of hematite in the ilmenite and the atomic Fe^{3+} content of the kleberite. This is illustrated in Fig. 5, where the atoms of Fe^{3+} in kleberite have been normalized by scaling [Ti] in kleberite to [Ti] in residual ilmenite (the assumption is that Ti remains immobile during the alteration process). Results from EMP analyses of composite Murray Basin kleberite grains from Grey and Li (2003) are included in Fig. 5. The points show considerable scatter, but they are grouped about a line of unit slope, and there is a clear trend of increasing Fe^{3+} in kleberite with increasing mole fraction of hematite in the parental ilmenite.

These observations are consistent with a mechanism of selective leaching of divalent metal oxides from ferrian ilmenite. The $R\bar{3}$ structure of ferrian ilmenite, $(\mathrm{FeTiO_3})_{1-x}(\mathrm{Fe_2O_3})_x$, consists of stacks of honeycomb-form $\mathrm{M_2O_3}$ layers of edge-shared octahedra along the *c* axis. The M atoms are ordered such that $(1-x)\mathrm{Ti}^{4+} + x\mathrm{Fe}^{3+}$ and $(1-x)\mathrm{Fe}^{2+} + x\mathrm{Fe}^{3+}$ occupy alternate layers (Harrison *et al*., 2000). Incorporation of $\mathrm{MgTiO_3}$, into ferrian ilmenite enhances the stability of the $R\bar{3}$ structure (Ghiorso, 1990), and so enhances the separation

TABLE 4. Electron-microprobe analyses (wt.%) for Königshain kleberite grains containing residual ilmenite.

	TiO_2	Fe_2O_3 *FeO	MgO	MnO	Al_2O_3	SiO_2	Total
Kleberite 1	60.9	21.3	2.25	0.28	2.15	0.55	87.4
Ilmenite 1	42.7	48.9	4.34	0.55	0.57	0.01	97.1
Kleberite 2	64.6	16.7	1.47	0.36	2.37	0.86	86.4
Ilmenite 2	44.2	46.9	4.62	0.79	0.64	0.0	97.2
Kleberite 3	64.8	11.9	0.39	0.08	4.98	2.46	84.6
Ilmenite 3	48.2	43.8	5.11	1.10	0.28	0.01	97.9
Kleberite 4	65.7	12.7	0.73	0.11	2.94	1.65	83.8
Ilmenite 4	44.6	46.2	5.66	0.41	0.63	0.01	97.5
Kleberite 5	70.4	11.3	0.45	0.11	2.15	1.10	85.5
Ilmenite 5	48.0	45.8	2.80	1.69	0.10	0.08	98.5
Kleberite 6	69.1	10.3	0.38	0.13	2.40	1.68	84.0
Ilmenite 6	47.4	44.5	4.77	1.36	0.33	0.02	98.4

Corresponding ilmenite compositions

	mol.% $FeTiO_3$	mol.% Fe_2O_3	mol.% $MgTiO_3$	mol.% $MnTiO_3$	mol.% Al_2O_3
Ilmenite 1	0.63	0.19	0.16	0.01	0.01
Ilmenite 2	0.63	0.17	0.17	0.02	0.01
Ilmenite 3	0.68	0.11	0.19	0.02	0
Ilmenite 4	0.60	0.17	0.21	0.01	0.01
Ilmenite 5	0.76	0.10	0.10	0.04	0
Ilmenite 6	0.71	0.09	0.18	0.02	0

* The Fe content is reported as Fe_2O_3 for kleberite and as FeO for ilmenite.

of high-valency strongly bonded metals and low-valency weakly bonded metals into different layers. For the residual MgO-rich ferrian ilmenite in the kleberite grains the compositions of the two layers are as follows:

Layer 1: $0.86\ Ti^{4+} + 0.14\ Fe^{3+}$
Layer 2:
$0.67\ Fe^{2+} + 0.17\ Mg^{2+} + 0.02\ Mn^{2+} + 0.14\ Fe^{3+}$

Selective leaching of the more weakly bonded layer 2 of divalent metal oxides (plus associated Fe^{3+} in layer 2) leaves the more strongly bonded layer 1 oxides, with an [Fe]:[Ti] atomic ratio of 0.14:0.86 $\equiv$ 1:6, which is the ratio in the associated kleberite. The reaction (grouping minor Mn with Mg) can be written:

$$(FeTiO_3)_{0.67}(MgTiO_3)_{0.19}(Fe_2O_3)_{0.14} + 2.14\ H^+ \rightarrow 0.143\ [FeTi_6O_{11}(OH)_5] + 0.67\ Fe^{2+} + 0.19\ Mg^{2+} + 0.137\ Fe^{3+} + 0.71\ H_2O$$

A similar reaction has been reported for kleberite formation in the Murray Basin deposits (Grey and Li, 2003). The small differences are due to the kleberite formula in Grey and Li (2003) not being normalized to 16 anions as in tivanite. The reaction involves predominantly direct leaching of divalent metal oxides, $MO + 2H^+ \rightarrow M^{2+} + H_2O$, together with minor proton exchange $M^{n+} \leftrightarrow nH^+$. The latter reaction results in hydroxyl ion incorporation in kleberite. The kleberite formation mechanism contrasts with that for pseudorutile formation, which involves a combination of oxidation and proton exchange

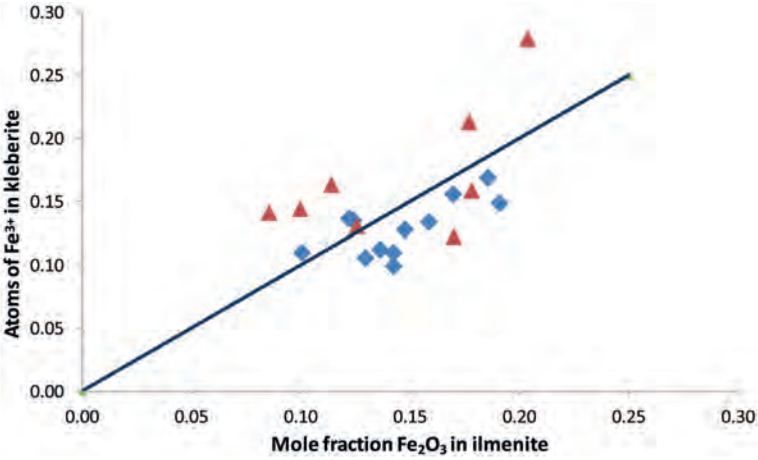

FIG. 5. Plot of the mol.% of hematite in residual MgO-rich ferrian ilmenite *vs*. the Fe^{3+} atomic content of the associated kleberite from EMP analyses of composite grains. The triangles indicate grains of Konigshain kleberite and the diamonds indicate grains of kleberite from the Murray Basin. The line has a slope of 1. The Fe^{3+} in kleberite has been scaled so that [Ti] in kleberite = [Ti] in the associated ilmenite.

(Ignatiev, 1999; Grey and Li, 2001). Pseudorutile formation leaves the [O]/[Ti] ratio unchanged, whereas kleberite formation involves oxygen removal and the [O]/[Ti] ratio decreases from 3.57 for the MgO-rich ferrian ilmenite to 2.67 for the mean kleberite composition.

It is evident from the kleberite formation reaction, described above, that MgO-rich ferrian ilmenite parent compositions with different hematite contents will produce kleberite with different [Fe]:[Ti] atomic ratios, which will lie along the line shown in Fig. 5. Scatter from the line, as shown in Fig. 5, is not surprising for natural systems, where incomplete leaching, as well as incorporation of iron-bearing impurities within the intragrain pores will move points above the line, and more extensive proton exchange for Fe^{3+} will move points below the line.

A question that remains to be resolved concerning the kleberite formation mechanism is whether the divalent metal oxides are selectively leached from the grains, or the whole matrix is dissolved and Ti^{4+} and Fe^{3+} are reprecipitated. The latter mechanism, known as a pseudomorphic replacement reaction (Putnis, 2002; Putnis and Putnis, 2007) is widespread in nature and in laboratory experiments. It is characterized by the preservation of the external shape and volume of the parent mineral, by a sharp reaction front between parent and product, and by extensive cracking and porosity in the product. These features are clearly present in the kleberite grains as shown in Fig. 1, as well as in figures of grains in Grey and Li (2003) and Grey *et al.* (2010). Information on whether selective leaching or interface-coupled dissolution-reprecipitation occurs could possibly be obtained by laboratory experiments involving ^{18}O exchange. Such experiments have recently been conducted on relatively pure natural ilmenite (Jannsen *et al.*, 2010), but they gave only rutile as product. It would be interesting to extend such studies to MgO-rich ferrian ilmenite grains.

Acknowledgements

We appreciate the help of Dr Ralf Thomas Schmitt, curator of minerals at the Museum für Naturkunde, Berlin, in providing a heavy mineral concentrate containing kleberite from Königshain. We thank Yesim Gozukara for conducting the TGA/DTA experiments. Thanks are also due to Cameron Davidson and Luda Malishev for EMP sample preparation.

References

Anand, R.R. and Gilkes, R.J. (1984) Weathering of ilmenite in a lateritic pallid zone. *Clays and Clay Minerals*, **32**, 363–374.

Anand, R.R. and Gilkes, R.J. (1985) Some alumina and silica in weathered ilmenite grains is present in clay minerals – a response to Frost *et al*. (1983). *Mineralogical Magazine*, **49**, 141–145.

Bautsch, H.J., Rohde, G., Sedlacek, P. and Zedler, A. (1978) Kleberit – Ein neues Eisen TitanOxidmineral aus Tertiaren Sänden. *Zeitschrift für Geologische Wissenschaften*, **6**, 661–671.

Frost, M.T., Grey, I.E., Harrowfield, I.R. and Mason, K. (1983) The dependence of alumina and silica contents on the extent of alteration of weathered ilmenites from Western Australia. *Mineralogical Magazine*, **47**, 201–208.

Ghiorso, M.S. (1990) Thermodynamic properties of hematite–ilmenite–geikelite solid solutions. *Contributions to Mineralogy and Petrology*, **104**, 645–667.

Grey, I.E. and Li, C. (2001) Low temperature roasting of ilmenite – phase chemistry and applications. *AusIMM Proceedings*, **306**, 35–42.

Grey, I.E. and Li, C. (2003) Hydroxylian pseudorutile derived from picroilmenite in the Murray Basin, southeastern Australia. *Mineralogical Magazine*, **67**, 733–747.

Grey, I.E. and Nickel, E.H. (1981) Tivanite, a new oxyhydroxide mineral from Western Australia, and its structural relationship to rutile and diaspore. *American Mineralogist*, **66**, 866–871.

Grey, I.E. and Reid, A.F. (1975) The structure of pseudorutile and its role in the natural alteration of ilmenite. *American Mineralogist*, **60**, 898–906.

Grey, I.E., Li, C. and Watts, J.A. (1983) Hydrothermal synthesis of goethite-rutile intergrowth structures and their relationship to pseudorutile. *American Mineralogist*, **68**, 981–988.

Grey, I.E., Watts, J.A. and Bayliss, P. (1994) Mineralogical nomenclature: pseudorutile revalidated and neotype given. *Mineralogical Magazine*, **58**, 597–600.

Grey, I.E., Bordet, P., Wilson, N.C., Townend, R., Bastow, T.J. and Brunelli, M. (2010) A new Al-rich hydroxylian pseudorutile from Kalimantan, Indonesia. *American Mineralogist*, **95**, 161–170.

Harrison, R.J., Redfern, S.A.T. and Smith, R.I. (2000) In-situ study of the $R\bar{3}$ to $R\bar{3}c$ phase transition in the ilmenite–hematite solid solution using time-of-flight neutron powder diffraction. *American Mineralogist*, **85**, 194–205.

Ignatiev, V.D. (1999) Solid-phase mechanism of the ilmenite leucoxenization. *Lithology and Mineral Resources*, **34**, 184–189.

Jannsen, A., Putnis, A., Geisler, T. and Putnis, C.V. (2010) The experimental replacement of ilmenite by rutile in HCl solutions. *Mineralogical Magazine*, **74**, 633–644.

Putnis, A. (2002) Mineral replacement reactions: from macroscopic observations to microscopic mechanisms. *Mineralogical Magazine*, **66**, 689–708.

Putnis, A. and Putnis, C.V. (2007) The mechanism of reequilibration of solids in the presence of a fluid phase. *Journal of Solid State Chemistry*, **180**, 1783–1786.

Rodriguez-Carvajal, J. (1990) *FULLPROF: A Program for Rietveld Refinement and Pattern Matching Analysis*. Satellite meeting on powder diffraction of the XV Congress of the IUCr, Toulouse, France, 27 pp.

Steinike, K. (2008) Der Kleberit im nordöstlichen Teil Deutschlands (1949–1990 Staatsgebiet der DDR). *Geohistorische Blätter*, **11**, 121–128.

Steinike, K. and Kaemmel, T. (2008) Kleberit – Pseudorutil/Hydroxy-Pseudorutil: zwei Welten – zwei Namen – ein Mineral? *Geohistorische Blätter*, **11**, 1–8.